

Impacts of various interfacial nanostructures on spectral phonon thermal boundary conductance

Cite as: J. Appl. Phys. **132**, 115108 (2022); <https://doi.org/10.1063/5.0106685>

Submitted: 29 June 2022 • Accepted: 27 August 2022 • Published Online: 19 September 2022

 Rui Xie,  Janak Tiwari and  Tianli Feng



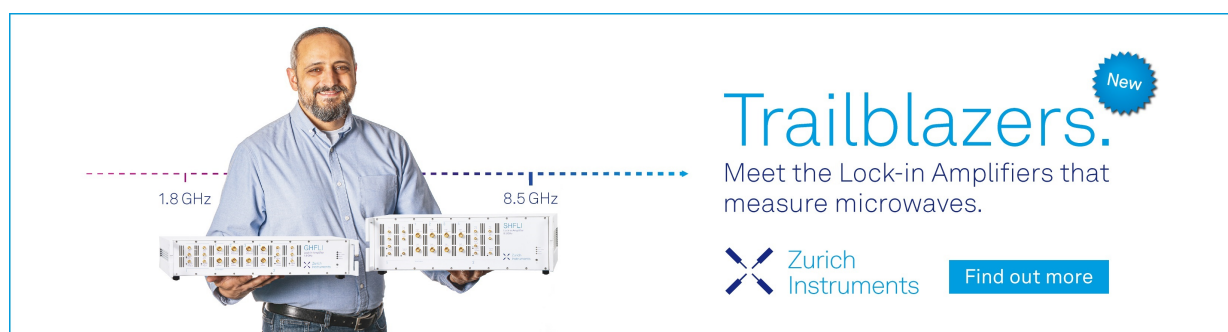
View Online




Export Citation




CrossMark



Trailblazers. 

Meet the Lock-in Amplifiers that measure microwaves.

 Zurich Instruments [Find out more](#)

Impacts of various interfacial nanostructures on spectral phonon thermal boundary conductance

Cite as: J. Appl. Phys. 132, 115108 (2022); doi: 10.1063/5.0106685

Submitted: 29 June 2022 · Accepted: 27 August 2022 ·

Published Online: 19 September 2022



Rui Xie,  Janak Tiwari,  and Tianli Feng^{a)} 

AFFILIATIONS

Department of Mechanical Engineering, University of Utah, Salt Lake City, Utah 84112, USA

^{a)}Author to whom correspondence should be addressed: tianli.feng@utah.edu

ABSTRACT

Nanoengineering of interfaces has become an effective way to tune the thermal boundary conductance (TBC) of heterostructures. However, the same nanostructure design can have opposite impacts on TBCs for different systems. To provide a clue toward a unified explanation, in this work, we directly and explicitly reveal the impacts of nanostructures on mode-dependent phonon TBC contributions. We study four representative types of nanostructures, i.e., (1) an intermediate layer, (2) interfacial interlaced teeth, (3) interfacial atomic mixing, and (4) interfacial atomic defects on two example heterostructures: $^{28}\text{Si}/\text{Ge}$ and $^6\text{Si}/\text{Ge}$, which have moderate and large phonon frequency mismatches, respectively. We find that most of these nanostructures reduce the TBC of $^{28}\text{Si}/\text{Ge}$ while increasing the TBC of $^6\text{Si}/\text{Ge}$. Each nanostructure is found to have two competing impacts on an interface—one tends to increase TBC while the other tends to decrease TBC. For example, adding an intermediate layer provides a phonon bridging effect, which tends to increase both elastic and inelastic phonon transmission, but it adds one more interface and, thus, more phonon reflection. As a result, an interlayer decreases the TBC of the $^{28}\text{Si}/\text{Ge}$ interface by decreasing the inelastic transmission while increasing both elastic and inelastic transmissions of the $^6\text{Si}/\text{Ge}$ interface. Other nanostructures with atomic disorder can increase transmission by increasing the contact area but can also decrease transmission by phonon-disorder backscattering. This work unveils the fundamental thermal transport physics across interfaces with nanostructures and sheds light on future interface nanoengineering for electronic devices such as high-power transistors, photodiodes, and supercomputing architectures.

Published under an exclusive license by AIP Publishing. <https://doi.org/10.1063/5.0106685>

I. INTRODUCTION

Heat flow management across material interfaces has become a major challenge for improving the performance of current devices ranging from large-scale engines and personal electronics to microprocessor chips and nanoscale transistors.^{1,2} Since the power density of electronic devices keeps increasing to satisfy the performance demand, the thermal management between nanoscale components becomes important.³ Thermal boundary conductance (TBC), which is a reciprocal of thermal resistance, plays an important role in the thermal management of electronic devices as it determines how difficult the heat flux can transport across interfaces.⁴

Nanoengineering of interfaces has been shown to be an effective way to tune the TBC of heterostructures.⁵ Various nanostructures, such as adding an intermediate layer,^{6–25} creating interlaced teeth,^{26–39} introducing interfacial atomic mixing,^{11,12,17,26,40–47} and introducing defects,⁴⁸ have been studied. However, their impacts on

TBC are diverse, i.e., the same nanostructure could lead to opposite impacts on different systems. Some examples are reviewed as follows.

Adding an intermediate layer has been extensively studied in the literature by simulations, and both improvement and decrease in TBCs are found in different scenarios.^{6–25} The first work was done by Hu *et al.* in 2010, who found that inserting water between the $\text{SiO}_2/\text{SiO}_2$ interface can enhance the TBC through non-equilibrium molecular dynamics (NEMD) simulations.⁶ They attributed the enhancement to the excellent match of vibrational states between trapped water and hydrophilic headgroups on two contact surfaces. After that, many other works have found increased TBC by adding an intermediate layer,⁶ and it is found that there is an optimal intermediate mass that gives the largest TBC improvement. For example, Le *et al.* found that the optimal mass is the geometric mean of the two materials, i.e., $m = \sqrt{m_A m_B}$.⁷ Liang *et al.* found that the optimum occurs at

$T_D = \sqrt{T_{DA}T_{DB}}$ by using NEMD simulations with Lennard-Jones (LJ) materials, where T_D is the Debye temperature.⁸ Saltonstall *et al.* found that the optimum occurs at $k^{-1} = (k_A^{-1} + k_B^{-1})/2$ or $m = (m_A + m_B)/2$ by using non-equilibrium Green's function (NEGF) with a 1D toy atomic chain, where k is the interatomic spring constant.⁹ Polanco *et al.* found that the optimum TBC occurs at $Z = \sqrt{Z_A Z_B}$ by a 1D atomic chain, where Z is the thermal impedance.¹⁰ Polanco *et al.* then revealed that the optimum occurs at $m = \sqrt{m_A m_B}$ by the NEGF method with a 3D toy crystal.¹¹ Some other very recent works further found that a graded intermediate mass can further improve the TBC compared to a single mass interlayer, and the optimal design is an exponential grading.^{12–15} However, several works have found that adding an interlayer could even decrease the TBC.^{7,16–19} For example, Liang *et al.* investigated the impact of an intermediate layer on the TBC between two toy Lennard-Jones (LJ) materials by NEMD simulations.¹⁶ They showed that the TBC could be improved when the two materials have a large mass mismatch and decreased when they have a moderate mismatch. They explained this as a competition between the increase in inelastic transmission and the decrease in elastic transmission, but no evidence or details are given. Most of the conclusions were made based on toy LJ materials, which do not have optical phonon modes and, thus, likely small inelastic phonon transmission, while the study on real systems like Si/Ge is rare.

Extensive experimental efforts have also been made to study the impact of adding intermediate layers.^{20–25} However, most works only focused on increasing TBC, and therefore, no decreasing TBC was reported. Most works explain the increase in the vibrational states' bridging effects and strengthening of interfacial chemical bonding.

Introducing interlaced teeth at interfaces has also been extensively studied in the literature.^{26–38} Most experimental and theoretical works found an increase in TBCs by interlaced teeth.^{26,29–31,35,37,38} They attribute the increase in TBC to the increase in the contact area. For example, in Ref. 37, the TBC is increased when nanopillars are introduced at the Al/Si interface, and the authors of Ref. 37 attributed this enhancement to the increase in the contact area. Note that in the TDTR measurement, the authors used a novel method. They deposited Al on the nanostructured Si surface by an electron-beam evaporator with a low deposit rate in order that the Al can fill the gap between Si pillars. The data fitting still assumed flat layers. At the same time, several theoretical works^{19,27,32–34,36} and experimental work²⁸ also found decreased TBC by interlaced teeth, which is attributed to diffuse scattering by the teeth. Despite these efforts, there is no clear phonon-level insight or evidence into the mechanisms, and it is still unpredictable whether the TBC will increase or decrease by interlaced teeth before doing molecular simulations.

Similarly, introducing interfacial atomic mixing has also been extensively studied in the literature.^{11,12,17,26,40–47} Most experimental and theoretical works found a decrease in TBCs by interfacial atomic mixing.^{12,26,41} They attribute the decrease in TBC to phonon atomic mixing scattering. At the same time, several theoretical works^{11,17,40,42–45} and experimental work⁴⁶ also found increased TBC by interfacial atomic mixing, which is attributed to the bridging effect.

Compared to the three structures discussed above, the impact of interfacial atomic defects is not very widely studied. Khosravian *et al.* found that vacancies in the Si/diamond interface can decrease the TBC by using NEMD simulations.⁴⁸ However, Giri *et al.* show that the introduction of nitrogen defects in the SiOC:H/SiC:H interface can increase the TBC. Similarly, Lu *et al.* found that vacancies in the Cu/Si interface can increase the TBC significantly by using NEMD simulations, i.e., 6.3% atomic vacancy increases 76% TBC.⁴⁹ Therefore, it is still not conclusive whether defects can enhance or decrease TBC, and there is no direct phonon-level insight into it.

To sum up, there is no unified theory to understand or predict the impact of different categories of nanostructures on TBC, and there is no universal principle or guidance on the design of nanostructures. Therefore, to provide insights into the reason for diverse impacts of various interfacial nanostructures on various systems, in this work, we study the impacts of four representative interfacial nanostructures on two different Si/Ge toy systems with mode-dependent phonon-level insights. The remainder of this paper is organized as follows. Section II describes the different nanostructural interfaces and methodology used in the study. Section III shows the TBC results for different interfaces. Section IV discusses the phonon mode analysis and provides a detailed explanation of the results presented in Sec. III. The conclusions are given in Sec. V.

II. METHODS

The four representative types of interfacial nanostructures studied in this work are shown in Fig. 1. The intermediate layer is shown in Fig. 1(a), with a thickness of 1.1 nm (2 unit cells). The interlaced teeth structure is shown in Fig. 1(b), with a length of 1.1 nm (2 unit cells) and a width of 0.8 nm (1.5 unit cells). In Fig. 1(c), the interfacial mixing is created by randomly mixing Si and Ge atoms in the region of 1.1 nm thickness. For the case of atomic defects, we use vacancies as an example and create three structures: (d) 10% vacancies randomly created on the Si side, (e) 10% vacancies randomly created on the Ge side, and (f) 10% vacancies randomly created on both sides.

To obtain the TBC for these structures, several methods can be used, such as the acoustic mismatch model (AMM),⁵⁰ diffuse mismatch model (DMM),^{51,52} atomistic Green's function (AGF),^{44,53,54} and molecular dynamics simulations. All first three methods only consider the carrier interactions within the harmonic approximation and do not take into account the inelastic processes. We note that a very recent work by Dai and Tian⁴⁷ included inelastic processes in AGF, but the computation is complicated. In this work, we choose NEMD simulation because it naturally considers all the orders of anharmonicity and inelastic processes. Also, MD simulations take into account the effect of interfacial modes, i.e., the process that “a mode of material A is converted into interfacial modes and then into a mode of material B,”⁵⁵ which cannot be captured by other methods.⁴ After NEMD simulations, the trajectories are used for the phonon mode-level analysis to extract the phonon mode-dependent contribution of TBC.

The NEMD simulations and mode-level phonon analysis setups are shown in Fig. 2. NEMD simulations were performed

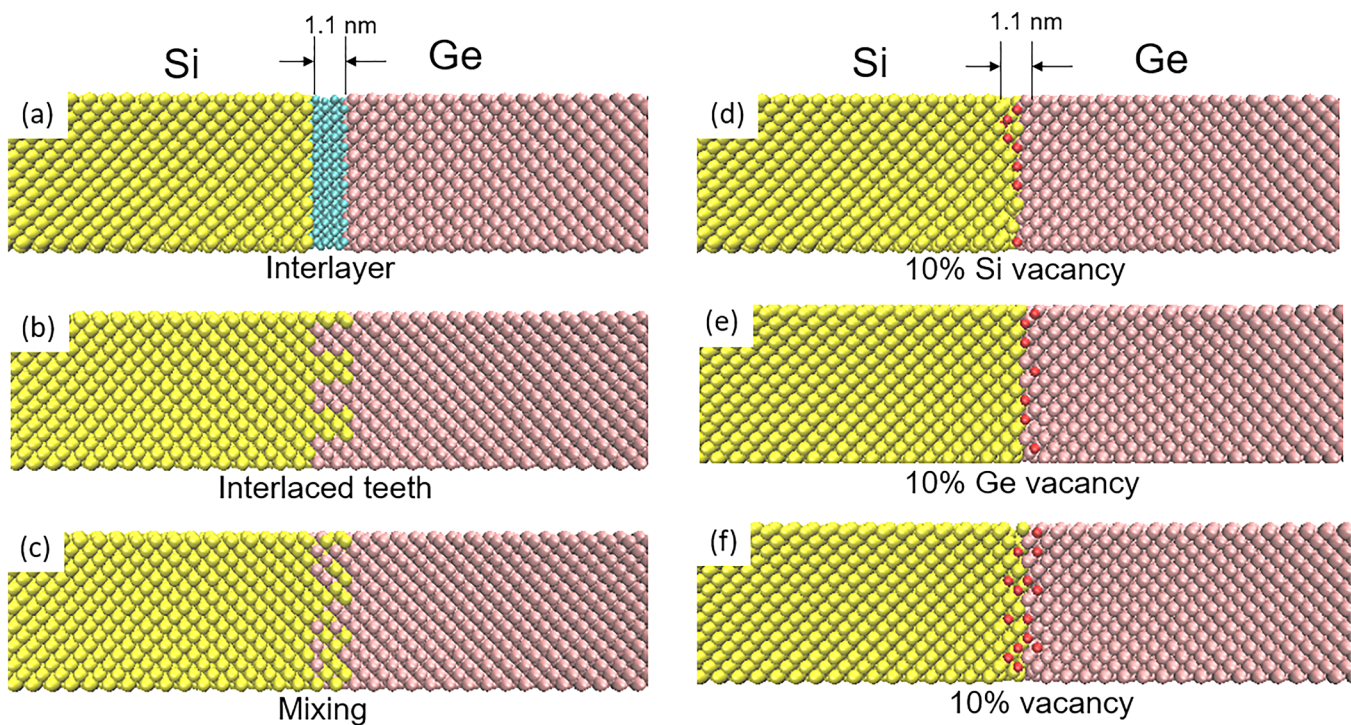


FIG. 1. Four representative types of interfacial nanostructures studied in this work. (a) Intermediate layer (interlayer). (b) Interlaced teeth. (c) Interfacial atomic mixing. (d) and (e) Atomic vacancies.

using the LAMMPS package^{56,57} with the Tersoff interatomic potential.^{58,59} Si and Ge have different lattice constants, and it is difficult to simulate the mismatched interface as it requires large cross section area. There are two methods to solve this problem. One is to use average lattice constant for both Si and Ge to enforce the same lattice constant. However, it will cause non-zero strain and will shake the whole system (see Ref. 4). The shake will add translational motion, which does not allow the spectral phonon

analysis to work properly. The other method is to change the potential of Ge to be the same as Si so that they have the same lattice constant. Therefore, we use both Si potential for both Si and Ge, and the simulated systems are essentially the Si/heavy Si interface. The size effect of NEMD simulations has been considered. Our model is the same as the ones in Ref. 4, which calculated the TBCs with different sizes. The results show that the TBCs are converged with the domain size of 152 nm, which is taken in this

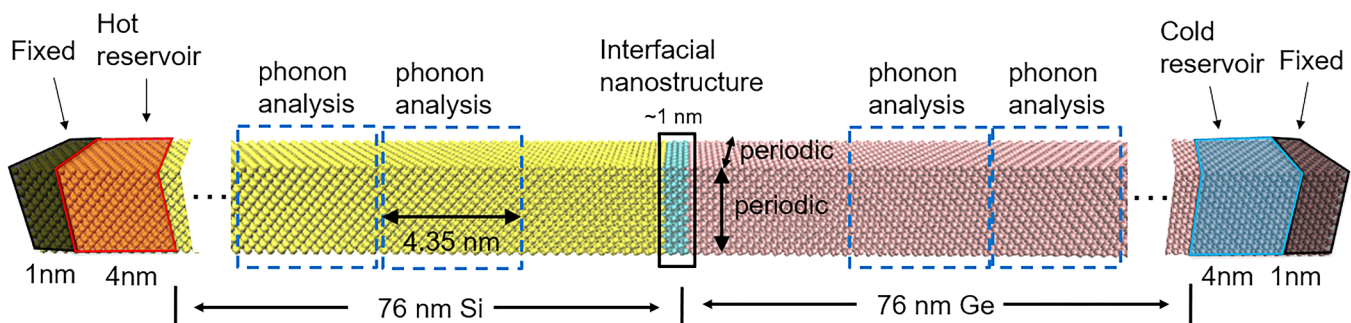


FIG. 2. NEMD simulation setup. Dimensions of the system, hot/cold reservoirs, and fixed boundaries are marked in the figures. The lateral dimensions are 4.35×4.35 nm (8×8 conventional cells), with periodic boundary conditions applied. Mode-level phonon analyses are done at different locations throughout the domain.

work, same as in Ref. 4. The TBCs in MD simulations are extracted by the following method. The heat flux is extracted by monitoring and averaging the energy gain and loss rates in cold and hot reservoirs, respectively. The temperature jump at the interface is extracted by linearly fitting the temperatures of the two bulk regions and extrapolating them to the middle line (i.e., interface location).

The mode (λ)-dependent phonon heat flux Q_λ is extracted from NEMD simulations by⁶⁰

$$Q_\lambda = \sum_{l,b}^{N_c,n} \left\langle \frac{1}{\sqrt{N_c m_b}} [E_{l,b}(t) - S_{l,b}(t)] \mathbf{e}_{b,\lambda} e^{i\mathbf{k} \cdot \mathbf{r}_{lb}^0} \dot{\Phi}_\lambda(t) \right\rangle, \quad (1)$$

where $\dot{\Phi}_\lambda(t)$ is the time derivative of the normal mode amplitude,⁶¹

$$\dot{\Phi}_\lambda(t) = \frac{1}{\sqrt{N_c}} \sum_{l,b}^{N_c,n} \sqrt{m_b} e^{-i\mathbf{k} \cdot \mathbf{r}_{lb}^0} \mathbf{e}_{b,\lambda}^* \cdot \dot{\mathbf{u}}_{l,b}(t), \quad (2)$$

which transforms the real-space atomic motions into phase-space phonon mode amplitudes. In Eq. (1), Q is the phonon heat flux vector. In our simulations, the heat flow is along the x direction, i.e., $Q_\lambda = (Q_{\lambda,x}, 0, 0)$. The subscript λ stands for a phonon mode (\mathbf{k}, ν) with \mathbf{k} and ν representing the phonon wave vector and the dispersion branch, respectively. $\langle \rangle$ denotes the time average. $E_{l,b}$ and $S_{l,b}$ are the total energy and stress of the atom (l, b), respectively. l and b label the indices of the primitive cells and basis atoms with the total numbers represented by N_c and n , respectively. m, r , and $\dot{\mathbf{u}}$ are the mass, equilibrium position, and velocity vector, respectively. $\mathbf{e}_{b,\lambda}$ and $\mathbf{e}_{b,\lambda}^*$ are the eigenvector and its complex conjugate at the basis b for mode λ , respectively. Both are vectors. The mode (λ)-dependent phonon TBC is calculated via⁴

$$G_\lambda = \frac{Q_{\lambda,x}}{\Delta T_{\text{MD}}}, \quad (3)$$

where ΔT_{MD} is the overall temperature drop at the interface in NEMD simulations. Although different phonons have different temperature drops ΔT_λ at the interface,⁴ the calculation of G uses the overall temperature drop ΔT_{MD} assuming that the experiment measures the apparent thermal conductance. If decomposition is done correctly, the summation of the heat flux of all phonon modes should be equal to the heat flux obtained from the real space in MD simulations Q_{MD} ,

$$\frac{1}{N_k} \sum_{\lambda}^{3nN_k} Q_{\lambda,x} = \frac{1}{N_c} Q_{\text{MD}}, \quad (4)$$

where N_k is the total number of \mathbf{k} points. In this work, $16 \times 16 \times 16$ \mathbf{k} points are used to decompose the total heat flux. The Langevin thermostat is used since it produces equilibrium mode-dependent phonons inside the reservoirs while Berendsen and Nose-Hoover generate nonequilibrium phonon temperatures inside the reservoirs.⁵⁵ The simulation details are identical with Ref. 4. The choice of boxes to perform the modal phonon analysis was discussed in Ref. 4 in details and can be summarized in the following points.

(1) We intentionally take boxes ~ 4 nm away from the interface because the phonon modal analysis needs to avoid the interfacial phonon modes near the interface region, which is about 1 nm thick. (2) We have tried different sizes of boxes and the modal heat fluxes obtained are the same. (3) We take six boxes on each side, and each box contains $8 \times 8 \times 8$ conventional cells with 4096 atoms. The spectral phonon heat fluxes are consistent and are averaged among the six boxes in the final data report.

In the formalisms, the only input is the real-space trajectory of the atoms in the sampled domains obtained from NEMD simulations. To eliminate the fluctuation in MD, Eqs. (1) and (2) need to be averaged over a sufficiently long time. We limit our calculations to classical molecular dynamics, which assumes a classical thermostat. Since we focus on a single temperature and compare the relative change of TBC with structures rather than temperatures, we do not discuss the quantum effect in depth. More information about quantum correction of classical MD can be found in Refs. 62 and 63.

III. RESULTS

The TBC values of bare and engineered $^{28}\text{Si}/^{73}\text{Ge}$ and $^6\text{Si}/^{73}\text{Ge}$ interfaces obtained by NEMD simulations are shown in Fig. 3. The TBCs for bare interfaces are found to be 445 and 80 $\text{MW/m}^2\text{K}$, respectively. The value for $^{28}\text{Si}/^{73}\text{Ge}$ agrees well with 410 $\text{MW/m}^2\text{K}$ obtained by Ref. 15 using the Tersoff potential, and the smaller value of Ref. 15 is mainly due to the different potential they used with us.⁵⁵ The value for $^6\text{Si}/^{73}\text{Ge}$ is much smaller, which is understandable because it has a much larger phonon frequency mismatch.

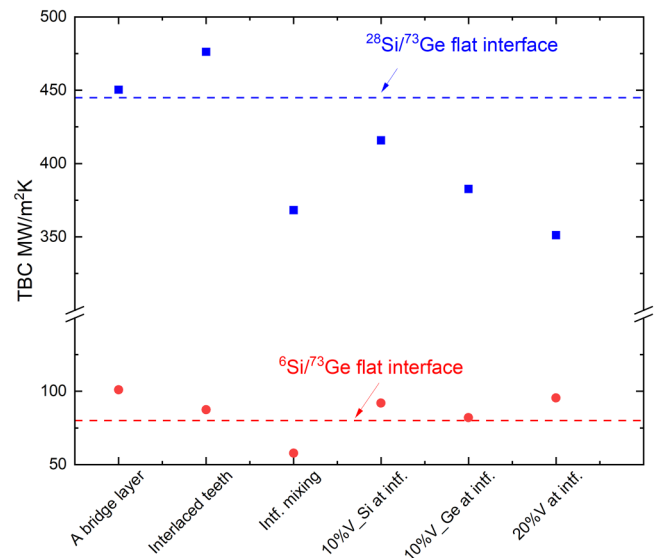


FIG. 3. TBC of the nanoengineered interfaces studied in this work. Blue squares represent $^{28}\text{Si}/^{73}\text{Ge}$ interfaces, and red circles represent $^6\text{Si}/^{73}\text{Ge}$ interfaces.

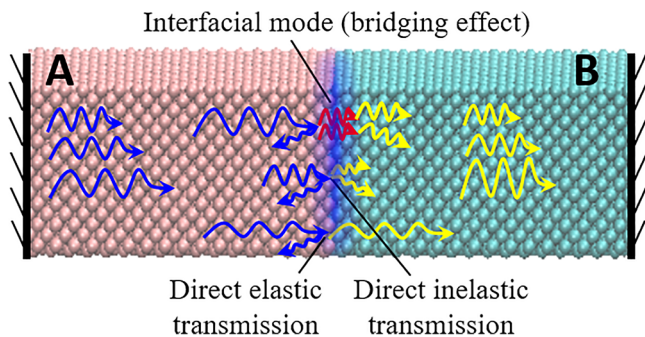


FIG. 4. Summary of phonon transmission mechanisms across an interface.

For $^{28}\text{Si}/^{73}\text{Ge}$ interface, all interfacial nanostructures (except interlaced teeth) decrease the TBC. However, for the $^{6}\text{Si}/^{73}\text{Ge}$ interface, all interfacial nanostructures (except interfacial atomic mixing) increase the TBC. Specifically, for $^{28}\text{Si}/^{73}\text{Ge}$, the interlaced teeth increase the TBC to $472 \text{ MW/m}^2 \text{ K}$ while the ^{50}Si interlayer, interfacial mixing, and 10% vacancy decrease the TBCs to 420, 367, and $347 \text{ W/m}^2 \text{ K}$, respectively. For $^{6}\text{Si}/^{73}\text{Ge}$, the atomic mixing decreases the TBC to $56 \text{ MW/m}^2 \text{ K}$ while the ^{14}Si interlayer, interlaced teeth, and 10% vacancy increase TBCs to 112, 84, and $93 \text{ MW/m}^2 \text{ K}$, respectively. We can find that the same nanostructure could lead to opposite impacts on $^{28}\text{Si}/^{73}\text{Ge}$ and $^{6}\text{Si}/^{73}\text{Ge}$. This is consistent with what has been found in the literature, i.e., various impacts of nanostructures were found for different systems. In the following sections, we will try to reveal the underlying mechanisms by using phonon heat flux decomposition.

IV. DISCUSSIONS

As shown in Fig. 4, when a phonon arrives at an interface, it can (i) transmit through the interface while preserving its frequency,

(ii) transmit through the interface while changing its frequency by combining with other phonons and/or splitting into several phonons, or (iii) be reflected back. These transmission processes may be mediated by intermediate interfacial modes. These processes are generally dependent on the materials and interfacial properties in the following aspects: (1) elastic phonon transmission that is positively correlated with phonon DOS overlap, (2) inelastic phonon transmission mediated by lattice anharmonicity, defects, and intermediate interfacial modes, (3) phonon transmission that is proportional to the interfacial contacting area, (4) phonon backscattering by the interface or defects, and (5) phonon transmission affected by the strength of interface chemical bonding. Introducing an interfacial nanostructure may affect multiple factors in the same or opposite directions, resulting in an increase or decrease in TBC. In Secs. IV A–IV D, we will discuss the impacts of different interfacial nanostructures separately. The impacts are summarized in Tables I and II.

A. Impact of insertion of interlayer

First, we look into the impacts of the interlayer. As shown in Fig. 5, we obtain the TBCs of $^{28}\text{Si}/\text{M}/^{73}\text{Ge}$ and $^{6}\text{Si}/\text{M}/^{73}\text{Ge}$ interfaces, with various interlayer masses “M.” For $^{28}\text{Si}/\text{M}/^{73}\text{Ge}$, most masses reduce the TBCs. The minimum occurs when $M \approx 50$, with a 5.6% reduction. In contrast, for $^{6}\text{Si}/\text{M}/^{73}\text{Ge}$, most masses increase the TBCs, and the maximum occurs at $M \approx 14$, with a 40% increase. To confirm that this is not a special case for the interlayer thickness we used, we have also conducted simulations for different interlayer thicknesses, as shown in Fig. 6. It is confirmed that the interlayers increase the TBC of $^{6}\text{Si}/^{73}\text{Ge}$ but decrease the TBC of $^{28}\text{Si}/^{73}\text{Ge}$. We note that recently Ma *et al.* did similar NEMD simulations for $^{28}\text{Si}/\text{M}/^{73}\text{Ge}$, and they found that TBC can be increased by adding ^{45}Si interlayers.¹⁵ The difference between their results and ours is probably we use a newer and more accurate Tersoff potential^{58,59} while Ref. 15 used an older Tersoff potential.⁶⁴

TABLE I. Summary of impacts of materials and interfacial properties on phonon transmission in different aspects. ✓ and ✗ represent increase and reduction in phonon transmission.

	(1) Elastic phonon transmission that is positively correlated with phonon DOS overlap (including interfacial modes)	(2) Inelastic transmission mediated by lattice anharmonicity, defects, and intermediate interfacial modes	(3) Elastic and inelastic transmission that are proportional to interfacial contacting area	(4) Elastic and inelastic transmission that are negatively related to backscattering by interface or defects	(5) Elastic and inelastic transmission affected by the strength of interface chemical bonding	Overall
$^{28}\text{Si}/\text{M}/^{73}\text{Ge}$	✓	✗✗	...	✗✗	...	✗
$^{6}\text{Si}/\text{M}/^{73}\text{Ge}$	✓✓	✓	...	✗✗	...	✓
$^{28}\text{Si}/\text{teeth}/^{73}\text{Ge}$	✓	✓	✓✓	✗	...	✓
$^{6}\text{Si}/\text{teeth}/^{73}\text{Ge}$	✓	✓	✓✓	✗	...	✓
$^{28}\text{Si}/\text{mixing}/^{73}\text{Ge}$	✓	✓	...	✗✗✗	...	✗
$^{6}\text{Si}/\text{mixing}/^{73}\text{Ge}$	✓	✓	...	✗✗✗	...	✗
$^{28}\text{Si}/\text{vacancy}/^{73}\text{Ge}$...	✓	...	✗✗	...	✗
$^{6}\text{Si}/\text{vacancy}/^{73}\text{Ge}$	✓	✓✓	...	✗	...	✓

TABLE II. Summary of impacts of materials and interfacial properties on elastic and inelastic phonon transmissions. ✓ and ✗ represent increase and reduction in phonon transmission.

	Elastic phonon transmission	Inelastic phonon transmission	Overall
$^{28}\text{Si}/\text{M}/^{73}\text{Ge}$	✓	✗✗	✗
$^6\text{Si}/\text{M}/^{73}\text{Ge}$	✓✓	✓	✓
$^{28}\text{Si}/\text{teeth}/^{73}\text{Ge}$	✓	✓	✓
$^6\text{Si}/\text{teeth}/^{73}\text{Ge}$	✓	✓	✓
$^{28}\text{Si}/\text{mixing}/^{73}\text{Ge}$	✗	✗	✗
$^6\text{Si}/\text{mixing}/^{73}\text{Ge}$	✗	✗	✗
$^{28}\text{Si}/\text{vacancy}/^{73}\text{Ge}$	✗	✗	✗
$^6\text{Si}/\text{vacancy}/^{73}\text{Ge}$	✓	✓	✓

To find out the reason why interlayer reduces TBC of $^{28}\text{Si}/^{73}\text{Ge}$ but increases TBC of $^6\text{Si}/^{73}\text{Ge}$, we first review similar studies with interlayers in the literature. We find that most literature works only found an increasing trend of TBC by adding an interlayer. They explain this by the phonon bridging effect, in which the interlayer phonon DOS bridges the vibration spectra of the two materials. Several other works have found either an increase or a decrease in TBCs, and they explained this as a competition between the increase in inelastic transmission and the decrease in elastic transmission, but no evidence or details are given.

To gain more direct insight, we calculate TBC contributions from individual phonon modes in $^{28}\text{Si}/\text{M}/^{73}\text{Ge}$ and $^6\text{Si}/\text{M}/^{73}\text{Ge}$ interfaces, as shown in Fig. 7. The total TBCs summed from modal

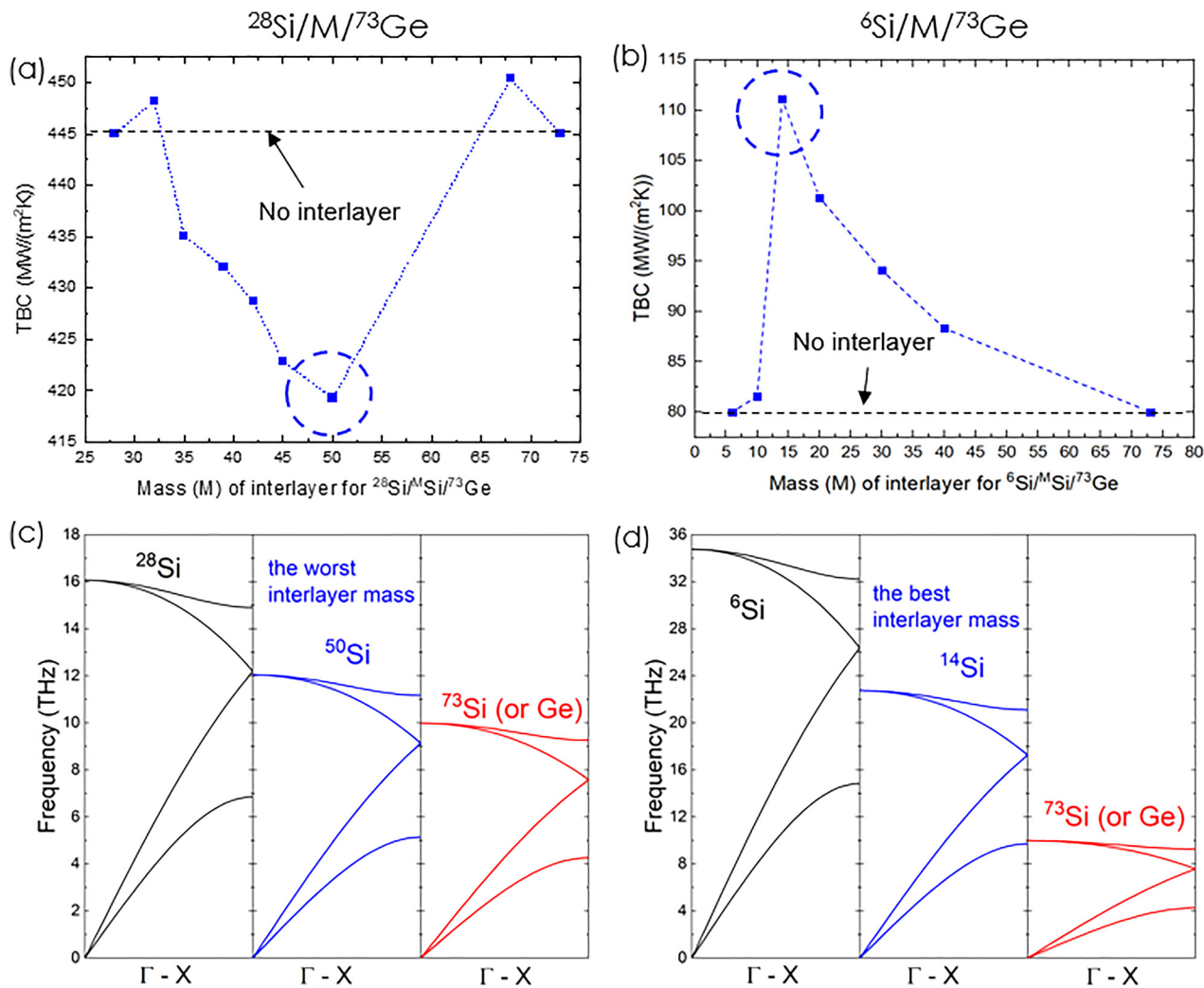


FIG. 5. Thermal boundary conductance of $^{28}\text{Si}/\text{M}/^{73}\text{Ge}$ and $^6\text{Si}/\text{M}/^{73}\text{Ge}$ as a function of interlayer's mass M: (a) TBC of $^{28}\text{Si}/\text{M}/^{73}\text{Ge}$ as a function of mass M; (b) TBC of $^6\text{Si}/\text{M}/^{73}\text{Ge}$ as a function of mass M; (c) phonon dispersion of ^{28}Si , ^{50}Si , and ^{73}Si (or Ge); (d) phonon dispersion of ^6Si , ^{14}Si , and ^{73}Si (or Ge).

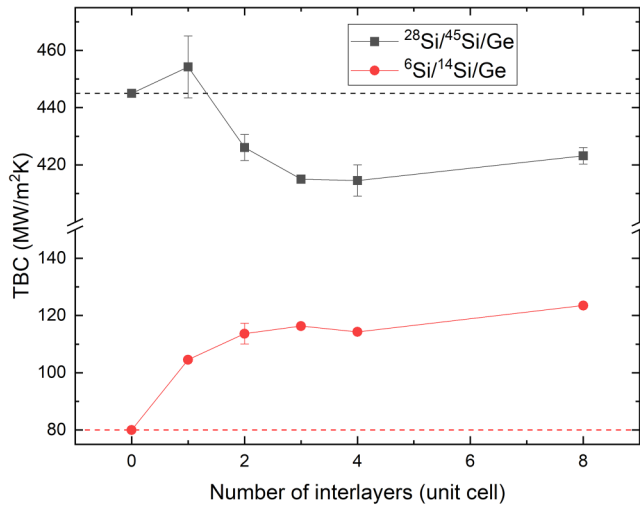


FIG. 6. Thermal boundary conductance of $^{28}\text{Si}/^{45}\text{Si}/^{73}\text{Ge}$ and $^6\text{Si}/^{14}\text{Si}/^{73}\text{Ge}$ as a function of interlayer's thickness. The thickness of a unit cell is about 0.5442 nm.

contributions in the full BZ match very well with the TBC values from real space calculation, suggesting that the mode-level phonon heat flux decomposition is done correctly. From the figure, a clear increase in acoustic phonon (low frequency) contribution after inserting an interlayer is found, but the optical phonons' change is buried in the figure. To have a clear view of the change in optical phonon contributions, we plot the TBC accumulation as a function of frequency in Fig. 8.

Figure 8(a) shows the TBC accumulations for $^{28}\text{Si}/\text{Ge}$ and $^{28}\text{Si}/^{50}\text{Si}/\text{Ge}$ interfaces. The difference between them is shown in Fig. 8(b). It is clearly seen that the acoustic phonons below 5 THz have an increased contribution after inserting the interlayer, but the high-frequency phonons' contribution is largely decreased, overwhelming the increase in acoustic phonons, resulting in a decrease in total TBC. We use green, red, and blue colors to label whether the phonons' TBC contribution is increased, decreased, or unchanged after inserting the interlayer in Fig. 8(c), respectively. It is seen that the ^{50}Si interlayer enhances the low-frequency elastic transmission but decreases the high-frequency inelastic transmission. The enhancement of low-frequency elastic transmission is understandable because the interlayer provides an intermediate phonon DOS to bridge the two materials, which can enhance

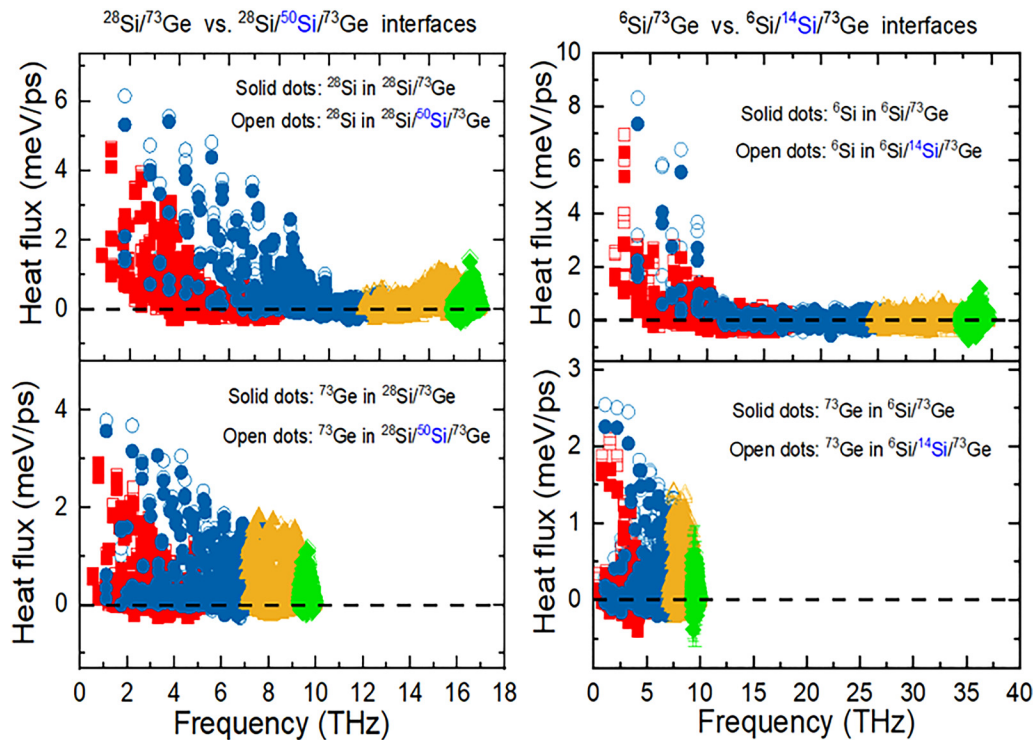


FIG. 7. The phonon contribution to TBC from each phonon mode. (left) $^{28}\text{Si}/^{73}\text{Ge}$ and $^{28}\text{Si}/^{50}\text{Si}/^{73}\text{Ge}$ interfaces. (right) $^6\text{Si}/^{73}\text{Ge}$ and $^6\text{Si}/^{14}\text{Si}/^{73}\text{Ge}$ interfaces.

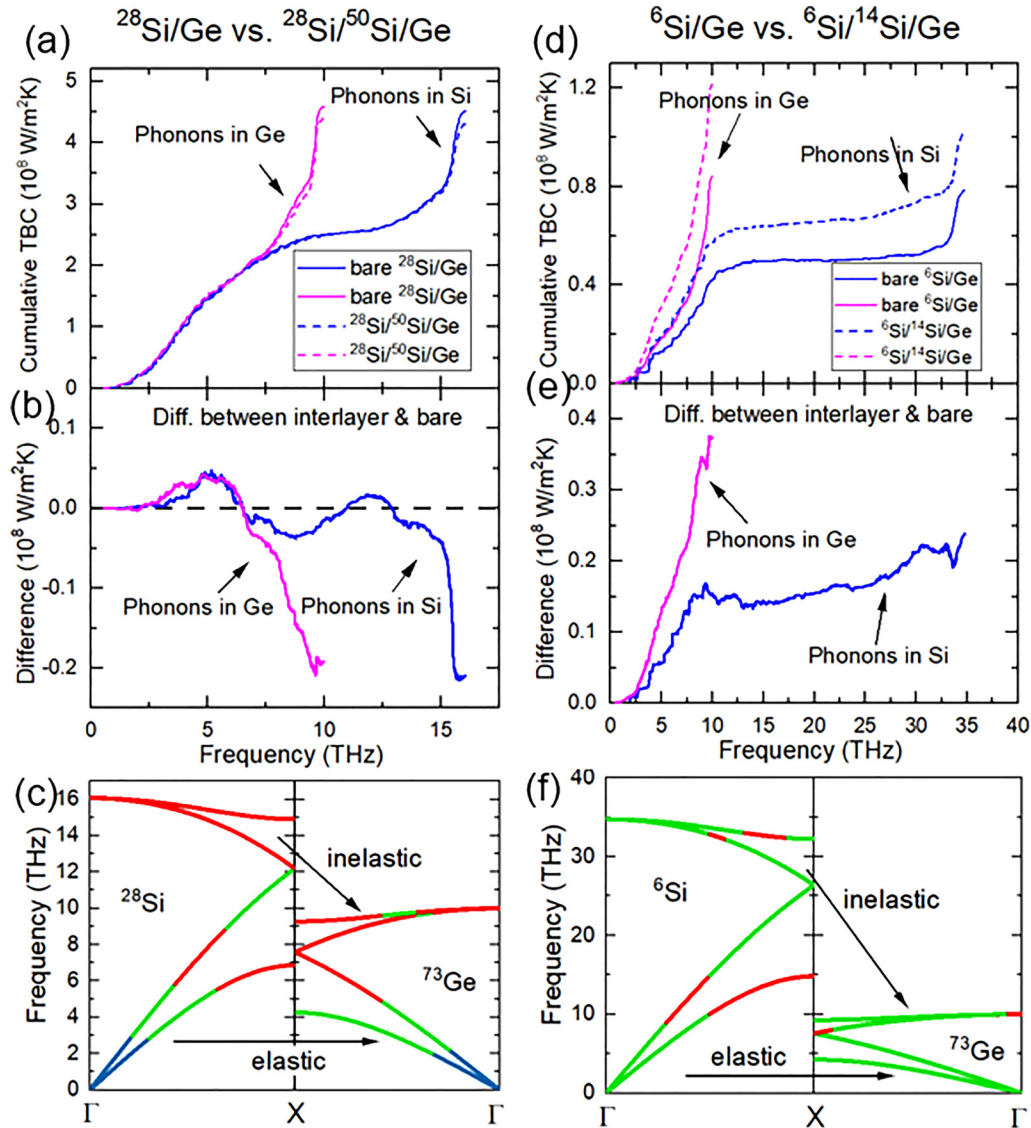


FIG. 8. Impacts of the interlayer on the spectral phonon contribution to TBC. (a) Cumulative phonon TBC of $^{28}\text{Si}/\text{Ge}$ and $^{28}\text{Si}/^{50}\text{Si}/\text{Ge}$ interfaces. (b) The difference between cumulative TBCs in $^{28}\text{Si}/^{50}\text{Si}/\text{Ge}$ and $^{28}\text{Si}/\text{Ge}$ interfaces. (c) Change of phonon TBC in phonon dispersion. Blue: phonon TBC does not change after introducing the interlayer. Green: phonon TBC enhanced. Red: phonon TBC decreased. (d)–(f) Same plots as (a)–(c) but for $^6\text{Si}/\text{Ge}$ and $^6\text{Si}/^{14}\text{Si}/\text{Ge}$ interfaces.

elastic transmission based on the acoustic mismatch model (i.e., one can prove that transmission $\frac{4Z_1Z_2}{(Z_1+Z)^2(Z+Z_2)^2} > \frac{4Z_1Z_2}{(Z_1+Z_2)^2}$, where $Z_1 < Z < Z_2$ are the acoustic impedances of the left, interlayer, and right materials, respectively). The decrease in the high-frequency inelastic transmission is due to two competing effects: (1) the interlayer phonon DOS bridging effect tends to increase the inelastic transmission, while (2) the increased reflection by adding one more interface by the interlayer tends to decrease the transmission. For comparison, similar plots for $^6\text{Si}/\text{Ge}$ and $^6\text{Si}/^{14}\text{Si}/\text{Ge}$ interfaces are shown in Figs. 8(d)–8(f). The interlayer increases both

low-frequency elastic transmission and high-frequency inelastic transmission. This indicates that the phonon DOS bridging effect dominates over additional reflection caused by adding an interface. These effects are summarized in Table I.

B. Impact of interlaced teeth

Second, we study the impact of interlaced teeth, and the results are shown in Fig. 9. It is found that for both $^{28}\text{Si}/^{73}\text{Ge}$ and $^6\text{Si}/^{73}\text{Ge}$, the interlaced teeth increase the overall elastic and

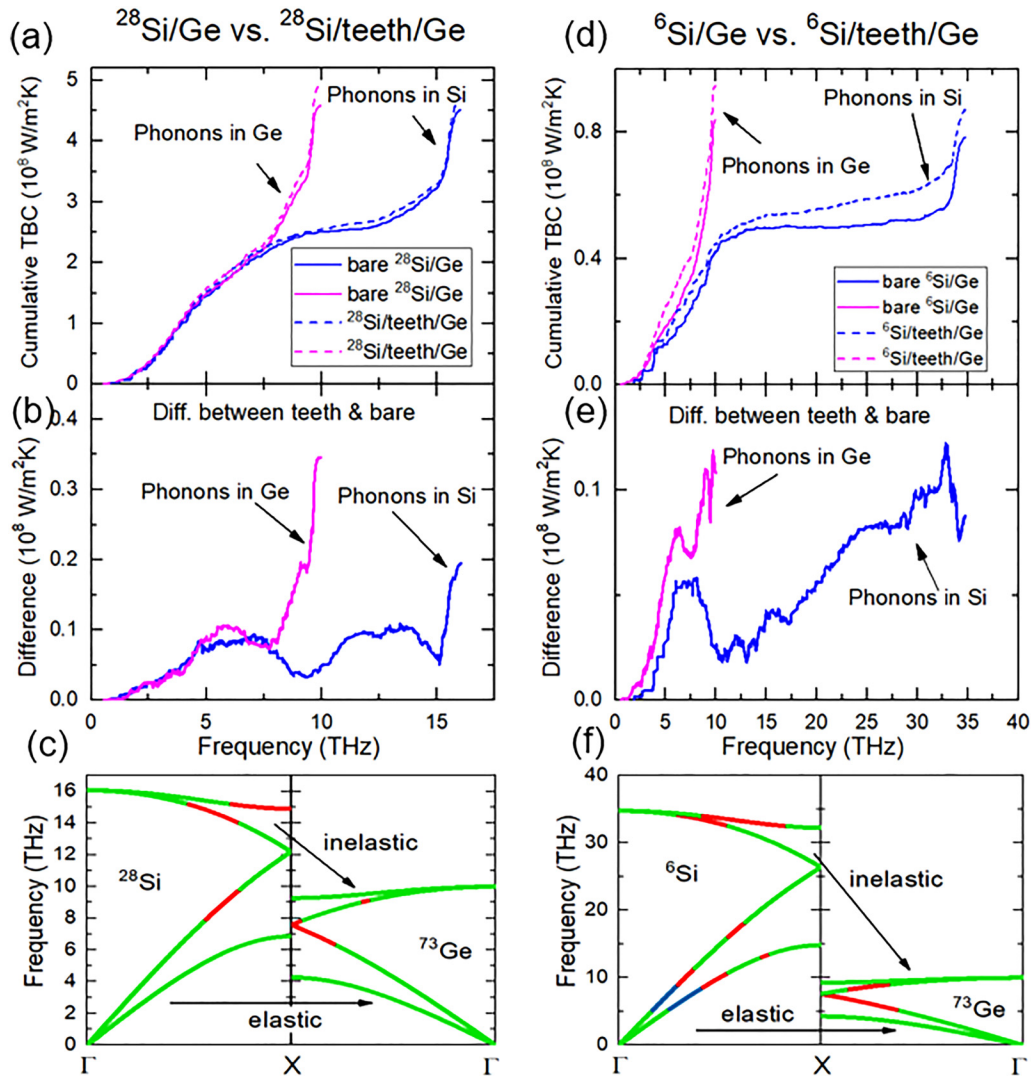


FIG. 9. Same plot as Fig. 8 but for the impact of interlaced teeth.

inelastic transmissions, although they have a decrease in some frequency ranges. The increase in TBC by interlaced teeth is found in many papers in the literature. For example, Sun *et al.*³⁶ and Zhou *et al.*²⁹ found that teeth can increase the interference of phonon and restore phonon transmission because of the contact area increase for Si/Ge and Al/GaN interfaces by NEMD. Jin *et al.* found that various teeth geometries can all enhance TBC.³⁵ At the same time, several papers find decreased TBC with interlaced teeth.³⁴ For example, Zhou *et al.*³⁴ found that the introduction of teeth induces more phonon scattering, which tends to decrease the phonon transmission, but it also provides additional phonon transport channels, which tend to increase the phonon transmission. These two factors compete with each other. As a result, TBC first decreases and then increases with increasing teeth area. If the teeth

area fraction is fixed, a larger total area and shorter teeth give larger TBC. In our case, the teeth length is about 1 nm, and the area ratio is about 0.5, which locates in the optimal range provided by Zhou *et al.*³⁴ The benefit provided by the increase in phonon transmission area dominates over backscattering by the increased contacting area, leading to the increase in overall TBC. The impacts of interlaced teeth are summarized in Table I.

C. Impact of interfacial atomic mixing

The interfacial atomic mixing is found to reduce the TBCs of both interfaces, e.g., by 18% for $^{28}\text{Si}/^{73}\text{Ge}$ and 30% for $^6\text{Si}/^{73}\text{Ge}$, respectively. Several other works have also found decreased TBCs for Si/Ge²⁶ and LJ solids¹² by using MD simulations. However, we

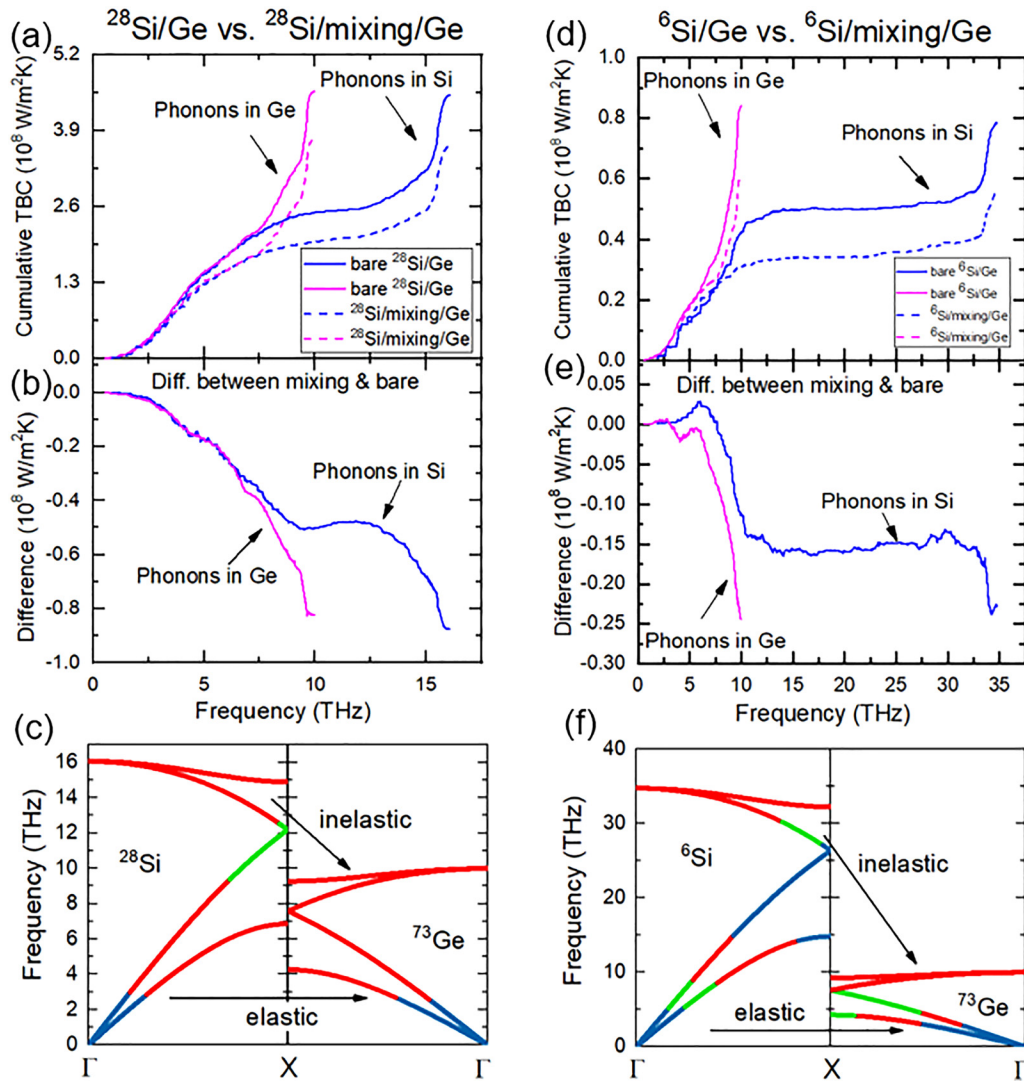


FIG. 10. Same plot as Fig. 8 but for the impact of interfacial atomic mixing.

noticed that there are many works that find increased TBCs by interfacial atomic mixing for Si/Ge,^{44,46,47} Al/Si,⁴⁵ and other solids^{11,40,42,43} by using various methods including Green's function and MD simulations. Interestingly, we find it is true that all the works reporting decreased TBCs share a common point: they all assume that the two solids only differ by atomic mass while sharing the same interatomic potential and the crystal structure. In contrast, all the works reporting increased TBCs are based on two solids with different interatomic potentials or interactions. Therefore, we suspect that the mass disorder only may not be able to increase phonon transmission, and it is the chemical bonding mixing that enhances the contact of the two materials and increases the phonon transmission.

The impact of interfacial atomic mixing on spectral phonon TBC is shown in Fig. 10. The contributions from both elastic and inelastic transmissions are decreased. We suspect that although mass disorder could provide a phonon vibrational bridge that tends to increase transmission, it also reflects or deflects the incoming phonons at the interface by phonon-point defect scattering. These factors are summarized in Table I.

Cheng *et al.*⁴⁶ realized the TBC measurement between Si and Ge for the first time, which is about $250 \text{ MW/m}^2\text{K}$. We notice that this value is smaller than our simulated result of $445 \text{ MW/m}^2\text{K}$ for the bare Si/Ge interface and $367 \text{ MW/m}^2\text{K}$ for the Si/mixing/Ge interface. Two possible reasons may account for this. First, we assume Ge and Si share the same potential and lattice constant

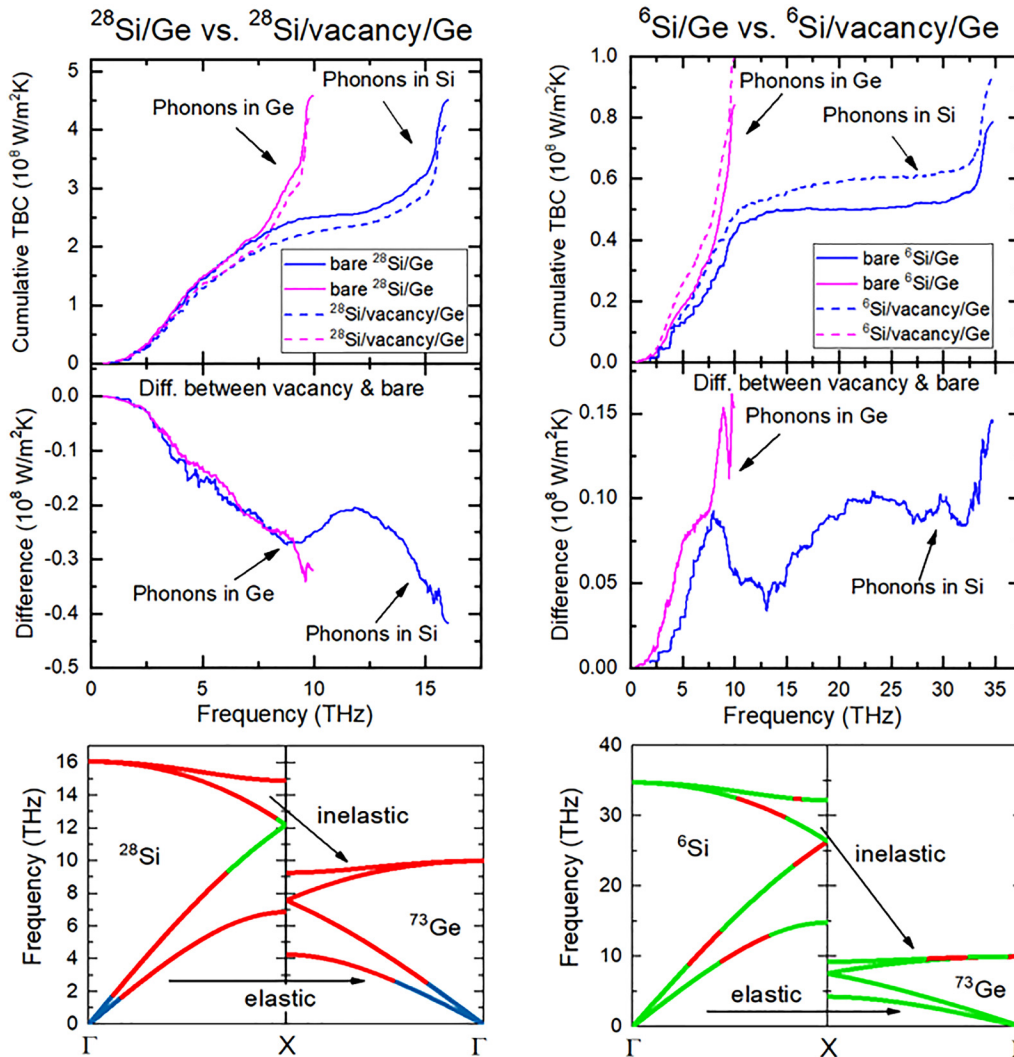


FIG. 11. Same plot as Fig. 8 but for the impact of interfacial atomic vacancies.

without strain, which may overestimate the phonon transmission across the interface. Second, the MD simulations use classical phonon statistics, which might overestimate the phonon specific heat compared to quantum statistics. In this work, we focus on self-consistent comparison and monitor the relative changes of TBC in various model systems. Therefore, the absolute TBC values should not be taken seriously, when being compared to the experiment.

D. Impact of interfacial vacancies

Finally, the impacts of 20% vacancy at the interfaces are studied. We find that the TBC is decreased by 22% in $^{28}\text{Si}/^{73}\text{Ge}$ but increased by 16% in $^6\text{Si}/^{73}\text{Ge}$. We note that, in the literature, the decreasing trend was also found in the Si/diamond interface,⁴⁸ while the increasing trend is also found in Cu/Si interfaces.⁴⁹

Khosravani *et al.* attributed the TBC decrease in Si/diamond interface⁴⁸ to the reflection of long-wavelength phonons by vacancies, which have high velocity and carry most of the heat. To verify this, we calculate the spectral phonon TBC contribution in Fig. 11. It is found that the acoustic phonons contribution is indeed decreased significantly in the $^{28}\text{Si}/^{73}\text{Ge}$ interface by vacancies. While for $^6\text{Si}/^{73}\text{Ge}$, which has a large phonon DOS mismatch, the vacancies can split the high-frequency phonons into low-frequency phonons and enhance inelastic transmission. This can explain the increase in TBC in Cu/Si as well.

V. CONCLUSIONS

To summarize, we have simulated Si/Ge interfaces with four different types of interfacial nanostructures, including an

intermediate layer, interlaced teeth, interfacial atomic mixing, and interfacial vacancies by using NEMD simulations and phonon spectral analyses. We find that each nanostructure can have two competing impacts—one tends to increase TBC while the other tends to decrease TBC. As a result, the same nanostructure design can have opposite impacts on TBCs for different systems. (1) Intermediate layer can introduce phonon DOS bridging effects, which tends to increase both elastic and inelastic transmission, but it also introduces one more interface and increases the phonon reflection. (2) Interlaced teeth increase the contact area, which increase both elastic and inelastic transmission channels, but they also provide more area for phonon reflection. (3) Interfacial atomic mixing increases phonon backscattering, resulting in a TBC decrease when the two materials are differed by atomic mass only. If the two materials are differed by interatomic potentials, the atomic mixing can increase the interface joining and increase the TBC. (4) The vacancies are found to decrease TBCs for materials with high sound velocity and increase TBCs for materials with low or largely mismatched sound velocities. Our conclusions are supported by mode-level phonon decomposition analysis results. This work pushes a step further toward the unification of impacts of various interfacial nanostructures on thermal boundary conductance, and it is expected to inspire more studies, which will have potentially large impacts on future electronic thermal management.

ACKNOWLEDGMENTS

We acknowledge support from the University of Utah and the Center for High Performance Computing.

AUTHOR DECLARATIONS

Conflict of Interest

The authors have no conflicts to disclose.

Author Contributions

Rui Xie: Investigation (lead); Methodology (supporting); Writing – original draft (equal). **Janak Tiwari:** Investigation (supporting); Writing – original draft (equal). **Tianli Feng:** Conceptualization (lead); Funding acquisition (lead); Methodology (lead); Project administration (lead); Supervision (lead); Writing – original draft (equal).

DATA AVAILABILITY

The data that support the findings of this study are available from the corresponding author on reasonable request.

REFERENCES

- ¹A. Shakouri, *Proc. IEEE* **94**, 1613 (2006).
- ²L. Shi, C. Dames, J. R. Lukes, P. Reddy, J. Duda, D. G. Cahill, J. Lee, A. Marconnet, K. E. Goodson, J. H. Bahk, A. Shakouri, R. S. Prasher, J. Felts, W. P. King, B. Han, and J. C. Bischof, *Nanoscale and Microscale Thermophysical Engineering* (Taylor and Francis Inc., 2015), pp. 127–165.
- ³A. L. Moore and L. Shi, *Mater. Today* **17**, 163 (2014).
- ⁴T. Feng, Y. Zhong, J. Shi, and X. Ruan, *Phys. Rev. B* **99**, 045301 (2019).
- ⁵A. Giri and P. E. Hopkins, *Adv. Funct. Mater.* **30**, 1903857 (2020).
- ⁶M. Hu, J. v. Goicochea, B. Michela, and D. Poulikakos, *Nano Lett.* **10**, 279 (2010).
- ⁷N. Q. Le, J. C. Duda, T. S. English, P. E. Hopkins, T. E. Beechem, and P. M. Norris, *J. Appl. Phys.* **111**, 084310 (2012).
- ⁸Z. Liang and H. L. Tsai, *Int. J. Heat Mass Transfer* **55**, 2999 (2012).
- ⁹C. B. Saltonstall, C. A. Polanco, J. C. Duda, A. W. Ghosh, P. M. Norris, and P. E. Hopkins, *J. Appl. Phys.* **113**, 013516 (2013).
- ¹⁰C. A. Polanco and A. W. Ghosh, *J. Appl. Phys.* **116**, 083503 (2014).
- ¹¹C. A. Polanco, R. Rastgarkafshgarkolaie, J. Zhang, N. Q. Le, P. M. Norris, P. E. Hopkins, and A. W. Ghosh, *Phys. Rev. B* **92**, 144302 (2015).
- ¹²Y. Zhou, X. Zhang, and M. Hu, *Nanoscale* **8**, 1994 (2016).
- ¹³C. A. Polanco, R. Rastgarkafshgarkolaie, J. Zhang, N. Q. Le, P. M. Norris, and A. W. Ghosh, *Phys. Rev. B* **95**, 195303 (2017).
- ¹⁴R. Rastgarkafshgarkolaie, J. Zhang, C. A. Polanco, N. Q. Le, A. W. Ghosh, and P. M. Norris, *Nanoscale* **11**, 6254 (2019).
- ¹⁵D. Ma, Y. Zhao, and L. Zhang, *J. Appl. Phys.* **129**, 175302 (2021).
- ¹⁶Z. Liang and H.-L. Tsai, *J. Phys.: Condens. Matter* **23**, 495303 (2011).
- ¹⁷T. S. English, J. C. Duda, J. L. Smoyer, D. a. Jordan, P. M. Norris, and L. v. Zhigilei, *Phys. Rev. B* **85**, 035438 (2012).
- ¹⁸E. Lee and T. Luo, *Phys. Chem. Chem. Phys.* **19**, 18407 (2017).
- ¹⁹L. Tao, S. Theruvakkattil Sreenivasan, and R. Shahsavari, *ACS Appl. Mater. Interfaces* **9**, 989 (2017).
- ²⁰X. Gu, C. Lee, J. Xie, E. Beam, M. Becker, T. A. Grotjohn, J. Anaya, M. Kuball, and W. R. Road, “GaN-on-diamond with ultra-low thermal barrier resistance,” (Qorvo Inc. Richardson, 2016), p. 405; available at <https://apps.dtic.mil/sti/citations/AD1025282>.
- ²¹Y. Zhou, J. Anaya, J. Pomeroy, H. Sun, X. Gu, A. Xie, E. Beam, M. Becker, T. A. Grotjohn, C. Lee, and M. Kuball, *ACS Appl. Mater. Interfaces* **9**, 34416 (2017).
- ²²L. Yates, J. Anderson, X. Gu, C. Lee, T. Bai, M. Mecklenburg, T. Aoki, M. S. Goorsky, M. Kuball, E. L. Piner, and S. Graham, *ACS Appl. Mater. Interfaces* **10**, 24302 (2018).
- ²³Z. Cheng, F. Mu, L. Yates, T. Suga, and S. Graham, *ACS Appl. Mater. Interfaces* **12**, 8376 (2020).
- ²⁴F. Mu, B. Xu, X. Wang, R. Gao, S. Huang, K. Wei, K. Takeuchi, X. Chen, H. Yin, D. Wang, J. Yu, T. Suga, J. Shiomi, and X. Liu, *J. Alloys and Compounds* **905**, 164076 (2022).
- ²⁵Y. Zhou, R. Ramaneti, J. Anaya, S. Korneychuk, J. Derluyn, H. Sun, J. Pomeroy, J. Verbeeck, K. Haenen, and M. Kuball, *Appl. Phys. Lett.* **111**, 041901 (2017).
- ²⁶L. Sun and J. Y. Murthy, *J. Heat Transfer* **132**, 102403 (2010).
- ²⁷M. Hu, X. Zhang, D. Poulikakos, and C. P. Grigoropoulos, *Int. J. Heat Mass Transfer* **54**, 5183 (2011).
- ²⁸P. E. Hopkins, L. M. Phinney, J. R. Serrano, and T. E. Beechem, in *2010 14th International Heat Transfer Conference, IHTC* (ASME, 2010), Vol. 6, p. 313.
- ²⁹X. W. Zhou, R. E. Jones, C. J. Kimmer, J. C. Duda, and P. E. Hopkins, *Phys. Rev. B* **87**, 094303 (2013).
- ³⁰S. Merabia and K. Termentzidis, *Phys. Rev. B* **89**, 054309 (2014).
- ³¹W. Park, A. Sood, J. Park, M. Asheghi, R. Sinclair, and K. E. Goodson, *Nanoscale Microsc. Thermophys. Eng.* **21**, 134 (2017).
- ³²Y.-C. Hua and B.-Y. Cao, *Int. J. Heat Mass Transfer* **154**, 119762 (2020).
- ³³X. Zhao, X. Qian, X. Li, and R. Yang, *J. Appl. Phys.* **129**, 215105 (2021).
- ³⁴Y. Xu, G. Wang, and Y. Zhou, *Int. J. Heat Mass Transfer* **187**, 122499 (2022).
- ³⁵S. Jin, Z. Zhang, Y. Guo, J. Chen, M. Nomura, and S. Volz, *Int. J. Heat Mass Transfer* **182**, 122014 (2022).
- ³⁶J. Sun, Y. Li, Y. Karaaslan, C. Sevik, and Y. Chen, *J. Appl. Phys.* **130**, 035301 (2021).
- ³⁷E. Lee, T. Zhang, T. Yoo, Z. Guo, and T. Luo, *ACS Appl. Mater. Interfaces* **8**, 35505 (2016).
- ³⁸E. Lee, T. Zhang, M. Hu, and T. Luo, *Phys. Chem. Chem. Phys.* **18**, 16794 (2016).
- ³⁹E. Lee, E. Mennerov, R. A. Hughes, S. Neretina, and T. Luo, *ACS Appl. Mater. Interfaces* **10**, 34690 (2018).

- ⁴⁰D. Kechrakos, *J. Phys.: Condens. Matter* **3**, 1443 (1991).
- ⁴¹G. Fagas, A. G. Kozorezov, C. J. Lambert, J. K. Wigmore, A. Peacock, A. Poelaert, and R. den Hartog, *Phys. Rev. B: Condens. Matter Mater. Phys.* **60**, 6459 (1999).
- ⁴²R. J. Stevens, L. v. Zhigilei, and P. M. Norris, *Int. J. Heat Mass Transfer* **50**, 3977 (2007).
- ⁴³H. Zhao and J. B. Freund, *J. Appl. Phys.* **105**, 013515 (2009).
- ⁴⁴Z. Tian, K. Esfarjani, and G. Chen, *Phys. Rev. B* **86**, 235304 (2012).
- ⁴⁵C. S. Gorham, K. Hattar, R. Cheaito, J. C. Duda, J. T. Gaskins, T. E. Beechem, J. F. Ihlefeld, L. B. Biedermann, E. S. Piekos, D. L. Medlin, and P. E. Hopkins, *Phys. Rev. B: Condens. Matter Mater. Phys.* **90**, 024445 (2014).
- ⁴⁶Z. Cheng, R. Li, X. Yan, G. Jernigan, J. Shi, M. E. Liao, N. J. Hines, C. A. Gadre, J. C. Idrobo, E. Lee, K. D. Hobart, M. S. Goorsky, X. Pan, T. Luo, and S. Graham, *Nat. Commun.* **12**, 6901 (2021).
- ⁴⁷J. Dai and Z. Tian, *Phys. Rev. B* **101**, 41301 (2020).
- ⁴⁸N. Khosravian, M. K. Samani, G. C. Loh, G. C. K. K. Chen, D. Baillargeat, and B. K. Tay, *J. Appl. Phys.* **113**, 024907 (2013).
- ⁴⁹Z. Lu, A. M. Chaka, and P. v. Sushko, *Phys. Rev. B* **102**, 075449 (2020).
- ⁵⁰W. Little, *Can. J. Phys.* **37**, 334 (1959).
- ⁵¹E. T. Swartz and R. O. Pohl, *Appl. Phys. Lett.* **51**, 2200 (1987).
- ⁵²E. Swartz and R. Pohl, *Rev. Mod. Phys.* **61**, 605 (1989).
- ⁵³W. Zhang, T. S. Fisher, and N. Mingo, *Numer. Heat Transfer Part B: Fundam.* **51**, 333 (2007).
- ⁵⁴N. Mingo and L. Yang, *Phys. Rev. B: Condens. Matter Mater. Phys.* **68**, 245406 (2003).
- ⁵⁵T. Feng, W. Yao, Z. Wang, J. Shi, C. Li, B. Cao, and X. Ruan, *Phys. Rev. B* **95**, 195202 (2017).
- ⁵⁶A. P. Thompson, H. M. Aktulga, R. Berger, D. S. Bolintineanu, W. M. Brown, P. S. Crozier, P. J. in 't Veld, A. Kohlmeyer, S. G. Moore, T. D. Nguyen, R. Shan, M. J. Stevens, J. Tranchida, C. Trott, and S. J. Plimpton, *Comput. Phys. Commun.* **271**, 108171 (2022).
- ⁵⁷S. Plimpton, *J. Comput. Phys.* **117**, 1 (1995).
- ⁵⁸J. Tersoff, *Phys. Rev. B* **38**, 9902 (1988).
- ⁵⁹J. Tersoff, *Phys. Rev. B* **39**, 5566 (1989).
- ⁶⁰Y. Zhou and M. Hu, *Phys. Rev. B* **95**, 115313 (2017).
- ⁶¹M. T. Dove, *Introduction to Lattice Dynamics* (Cambridge University Press, 1993).
- ⁶²J. E. Turney, A. J. H. McGaughey, and C. H. Amon, *Phys. Rev. B: Condens. Matter Mater. Phys.* **79**, 224305 (2009).
- ⁶³W. Lv and A. Henry, *New J. Phys.* **18**, 013028 (2016).
- ⁶⁴J. Tersoff, *Phys. Rev. Lett.* **56**, 632 (1986).